International Journal of
Molecular Sciences

MDPI

Article

Biased Allele-Specific Expression of the Triploid Rubber Tree Regulated Heterosis Related to Cold Tolerance

Cheng Zheng, Chenwanli Li, Jing Zhang, Yingfeng Niu and Changli Mao * and Jin Liu *

Yunnan Technology Innovation Center of Natural Rubber, Yunnan Key Laboratory of Sustainable Utilization Research on Rubber Tree, Yunnan Institute of Tropical Crops, Jinghong 666100, China
* Correspondence: maokangwan@163.com (C.M.); liujin06@126.com (J.L.)

Abstract

Allele-specific expression (ASE), the unequal expression of the two parental alleles at heterozygous loci, provides a direct molecular window into the regulatory divergence underlying heterosis in F1 hybrids. ASE to investigate heterosis in triploid rubber trees remained largely unexplored. In triploid rubber tree, where the maternal genome is present in two copies, this asymmetry takes on an additional layer of complexity. In this study, we established a time-resolved map of cold tolerance ASE for the triploid rubber tree to explore whether ASE in a cold-treated triploid rubber tree ($3n = 54$) reveals how the maternal and paternal bias genes divide their labour. Based on a trio-based variant calling and phasing pipeline, which included WASP-based mapping bias correction and beta-binomial statistical testing, we profiled ASE across four developmental time points related to cold tolerance. A total of 5030 genes with sufficient allele-specific coverage were analyzed; 2975 genes showed significant allelic imbalance, including 2258 maternal-biased and 717 paternal-biased genes. This finding revealed a genome-wide bias in expression dominance of 3.15:1, with a mean allelic read ratio of 0.606. We further identified 218 genes that were completely monoallelically expressed (144 maternal only and 74 paternal only), which represented prime candidates for cis-regulatory divergence and monoallelic-expression genes. Clustering of the time-course profiles separated the two directions of bias into functionally distinct programmes. Maternal-biased genes were enriched in housekeeping and biosynthetic processes, such as chloroplast function, histone modification, and protein and RNA binding. In contrast, paternal-biased genes were enriched in stress-responsive and regulatory pathways, including antibiotic and salicylic acid responses, spliceosome assembly, and transcription factor activity. This functional complementation suggested that the maternal genome drove core metabolism while the paternal genome contributed to stress adaptation, providing a mechanistic framework for heterosis in rubber trees. Our results established a comprehensive ASE landscape for the triploid rubber tree and highlighted monoallelic genes as priority targets for validating the molecular basis of hybrid vigor in triploid rubber trees.

Keywords: allele-specific expression; rubber tree; triploid; heterosis

Academic Editor: Intikhab Alam

Received: 13 October 2026
Revised: 12 November 2026
Accepted: 13 November 2026
Published: 26 November 2026

Copyright: © 2026 by the authors. Licensee MDPI, Basel, Switzerland. This article is an open access article distributed under the terms and conditions of the Creative Commons Attribution (CC BY) license.

1. Introduction

Heterosis and allele-specific expression (ASE) are closely linked phenomena in plant biology [1]. ASE, which denotes the unequal expression of gene alleles in diploid organisms, provides insights into how cis-regulatory and trans-regulatory variations influence gene expression in hybrids [2] and potentially contributes to heterosis [3]. In plants, ASE played a pivotal role in gene regulatory variation, heterosis, genomic imprinting, and adaptive evolution [4], and it sits at the centre of the three classical explanations of heterosis: under the dominance model, a functional allele from one parent masks a deleterious recessive allele from the other; under overdominance, the heterozygote outperforms either homozygote; under epistasis, interactions between loci inherited from different parents create novel, favourable combinations [5,6]. Each model makes a different prediction about allelic ratios, and ASE data can distinguish among them: consistent expression from the allele of the better parent supports dominance, shifts in the direction of bias between conditions point to overdominance, and complementary expression across pathways is the signature of epistasis [7,8]. Recent advancements in high-quality reference genomes. Haplotype-resolved assemblies [9,10], RNA-seq [11], ATAC-seq [12], single-nucleus or single-cell sequencing [13,14], and DNA methylation profiling [15] spurred a new wave of research that investigated ASE in various plant species.

Maize served as the most extensively studied system for connections between ASE and heterosis [16–18]. In heterozygous maize research, Pitz et al. showed nonadditive gene expression in partially heterozygous maize, providing direct evidence that the degree of heterozygosity modulated the extent of nonadditive expression [19]. Liu et al. traced the dynamics of gene and allelic expression during modern hybrid maize breeding, demonstrating how artificial selection reshaped allelic expression patterns over breeding cycles [20]. Beyond maize, ASE analysis has appeared in perennial crops. In Lotus, Gao et al. found that 36% of genes exhibited ASE in F1 lotus hybrids, with most bias favouring the tropical parent; cis-regulatory divergence explained most of the signal in flowers, leaves and rhizomes, and ASE genes were enriched for pathways tied to ecotypic divergence, such as rhizome enlargement and winter dormancy [21]. In tea, Wang et al. integrated ASE with ATAC-seq and showed that hybrids carry more accessible chromatin regions than their parents; maternal-biased genes, enriched for energy and terpenoid metabolism, and paternal-biased genes, enriched for glutathione metabolism, jointly contributed to heterosis [12]. In wheat, Wu et al. proposed a dual-engine model in which non-additive effects drive early growth vigour at anthesis while additive expression stabilises grain development at the filling stage; superior parental alleles accounted for more than 60% of non-additive genes, casting the better parent as an allelic reservoir [22]. ASE encompassed a spectrum ranging from slight allelic imbalance to complete monoallelic expression. In plants, it is usually detected by counting RNA-seq reads that carry each parental allele at heterozygous SNP sites in F1 hybrids [23]. ASE is measurable when the two alleles are distinguishable at heterozygous single nucleotide polymorphism (SNP) sites. Three factors determine the accuracy of such measurements: the reference genome, since a haplotype-resolved assembly eliminates mapping bias [10]; the alignment strategy, where a STAR + WASP combination reduces reference bias [24,25]; and the statistical framework, which in practice ranges from binomial and chi-square tests to DESeq2-based models. High-throughput RNA-seq technology has been widely used to measure ASE in various plant species. Studies on ASE and heterosis have been carried out in numerous crops; however, most of these studies have utilized customized approaches, posing challenges for cross-study comparisons. A recent review by Mattevi et al. rigorously evaluated 26 ASE analysis pipelines and singled out plant-specific obstacles-polyploidy, extensive heterozygosity, and large genome size as the main sources of disagreement [6].

The rubber tree (*Hevea brasiliensis*) represented the only commercially cultivated species for the production of natural rubber (cis-1,4-polyisoprene, rubber hydrocarbon) among roughly 2500 latex-producing plants [26]. The rubber tree thrived in tropical forests, where the critical temperature for its normal growth and development was 18 °C. In the rubber planting regions of Yunnan Province, low temperatures constituted the primary environmental factor that limited the growth, development, yield, and geographical planting [27,28]. The triploid rubber trees, which benefited from gene dosage effects, enhanced both rubber production and cold tolerance [29]. The triploid varieties 'Yunyan 77–2' and 'Yunyan 77–4', currently promoted and cultivated in Yunnan, demonstrated superior traits such as rapid growth, high yield, and strong cold resistance [30,31], thereby underscoring the significant research and development potential of triploid rubber tree breeding. The performance of 'Yunyan 77–2' and 'Yunyan 77–4' in various planting areas in Yunnan exceeded that of their diploid parent 'GT1' [32]. 'Yunyan 77–4', a triploid F1 hybrid ($3n = 54$) derived from a cross between the maternal parent 'GT1' ($2n = 36$) and the paternal parent 'PR107' ($2n = 36$), demonstrated that the $2n$ in triploid 'Yunyan 77–4' ($2n + n$) arose from the $2n$ female gametes of the maternal parent 'GT1', which experienced incomplete separation during meiosis second-division restitution (SDR) [33–35]. This study focused on elucidating the impact of ASE on heterosis. By analyzing ASE to investigate heterosis in triploid rubber trees, particularly regarding cold resistance, the research aimed to identify crucial candidate genes that govern cold resistance in triploids through the regulation of allele expression. This strategy provided a molecular foundation for the development of cold-resistant and high-yielding triploid rubber tree varieties in Yunnan.

2. Results

2.1. ASE Analysis Pipeline for Triploid Rubber Trees

ASE analysis primarily relied on RNA sequencing (RNA-seq) data, which compared the number of reads from two alleles to identify differentially expressed genes. ASE analysis encountered significant challenges due to reference-mapping bias; moreover, no reference haplotype genome existed for rubber tree triploids. Triploid rubber poses a particular problem: no haplotype-resolved reference exists for the triploid genotype, and reference bias can masquerade as maternal bias whenever reads match the maternal-reference genome more easily than the paternal alleles. In this study, the ASE identification process for rubber tree triploids, built a pipeline that moves from allele-specific variants (ASVs) to ASE genes (ASEGs) using parent-offspring resequencing together with RNA-seq (Figure 1a, Supplementary Figure S1).

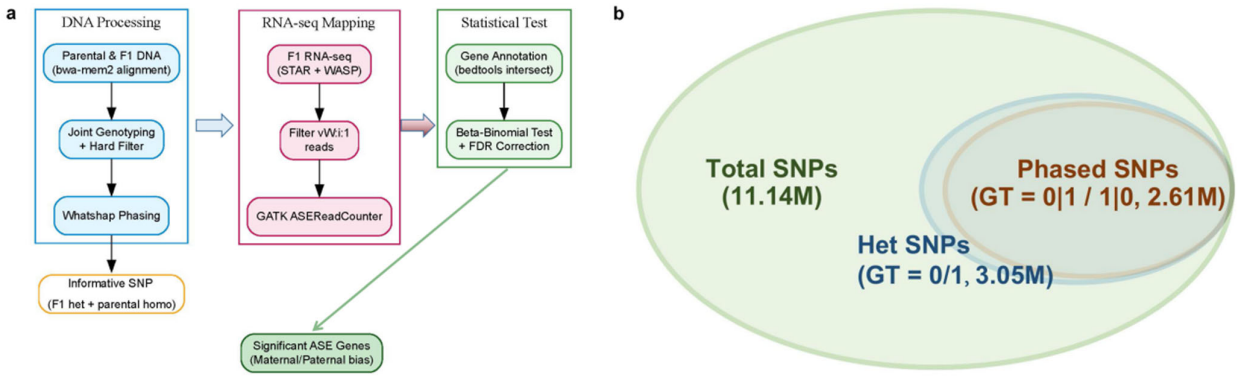
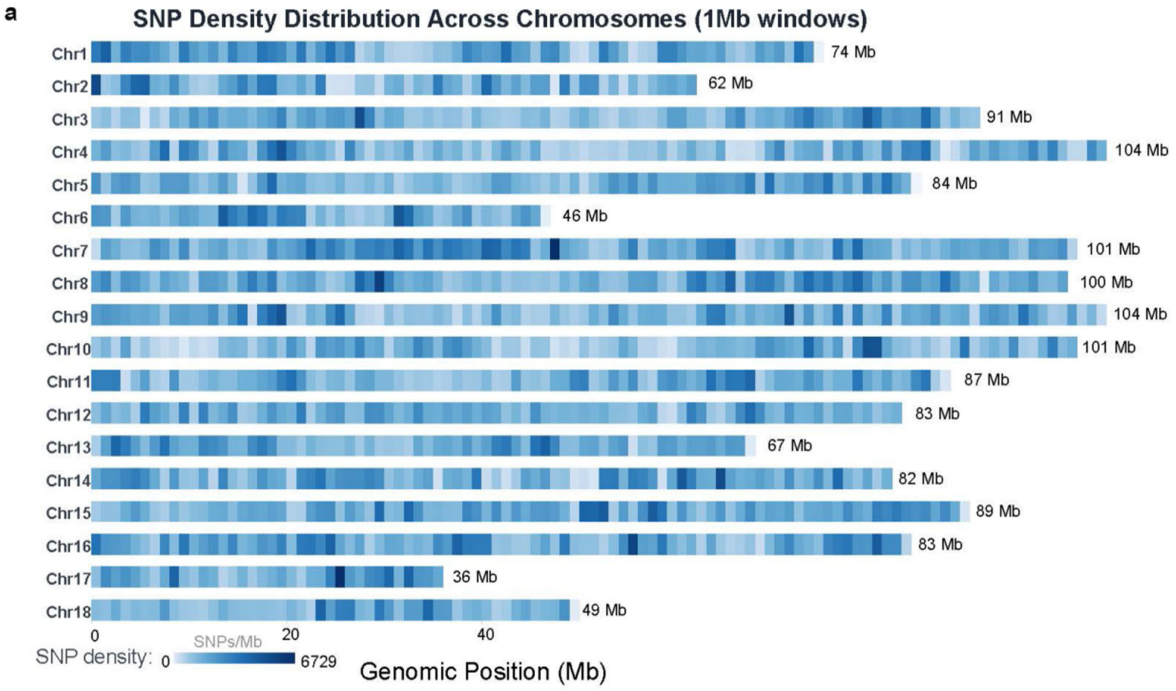


Figure 1. The triploid rubber tree ASE analysis pipeline. (**a**) ASE analysis pipeline. (**b**) Phasing heterozygous allele SNP.

Based on the resequencing data from the maternal parent 'GT1', the paternal parent 'PR107', and the F1 'Yunyan 77–4', we obtained a total of 11,144,572 SNPs by mapping to the reference genome and joint genotyping for SNP calling. Through phasing with whatshap, we identified a total of 2,608,663 heterozygous SNP sites that exhibited 0/1 phasing as either 1|0 or 0|1 (Figure 1b). The informative SNPs, obtained via the --varVCFfile option, were subsequently input into STAR to assess the bias of the RNA-seq reads.

2.2. Genome-Wide Landscape of ASE in Rubber Tree F1

The informative SNP density varied across the genome, and differences existed in the distribution density of ASE genes. To assess the genomic landscape of informative SNPs and ASE genes, the distribution and density of SNPs and ASE genes were calculated and visualized across 18 chromosomes of the rubber tree (Figure 2). The distribution of informative SNPs and ASE genes exhibited variation among the chromosomes. For informative SNPs, a minimum of 74,034 and a maximum of 211,088 SNPs were detected on chromosome 17 and chromosome 7, respectively. The average density of 1809 SNPs per Mb (Supplementary Table S2) across these 18 chromosomes ranged from 1436 (Chr 10) to 2098 (Chr 7). Regarding ASE genes, a minimum of 78 and a maximum of 580 ASEGs were identified on chromosome 17 and chromosome 15, respectively. Although chromosome 7 contained the most informative SNPs, chromosome 15 identified the highest number of ASE genes. Additionally, chromosome 15 harbored the largest number of 254 maternal bias genes, while chromosome 14 contained the 100 most paternal bias genes. The distribution of maternal and paternal bias genes varied across chromosomes. Maternal bias genes were most abundant on chromosome 15 and least abundant on chromosome 17, whereas paternal bias genes were most abundant on chromosome 14 and least abundant on chromosome 18. As illustrated in Figure 2a, maternal and paternal bias genes exhibited a certain linkage range on chromosomes; however, the specific causes of this formation required further investigation through additional analysis.



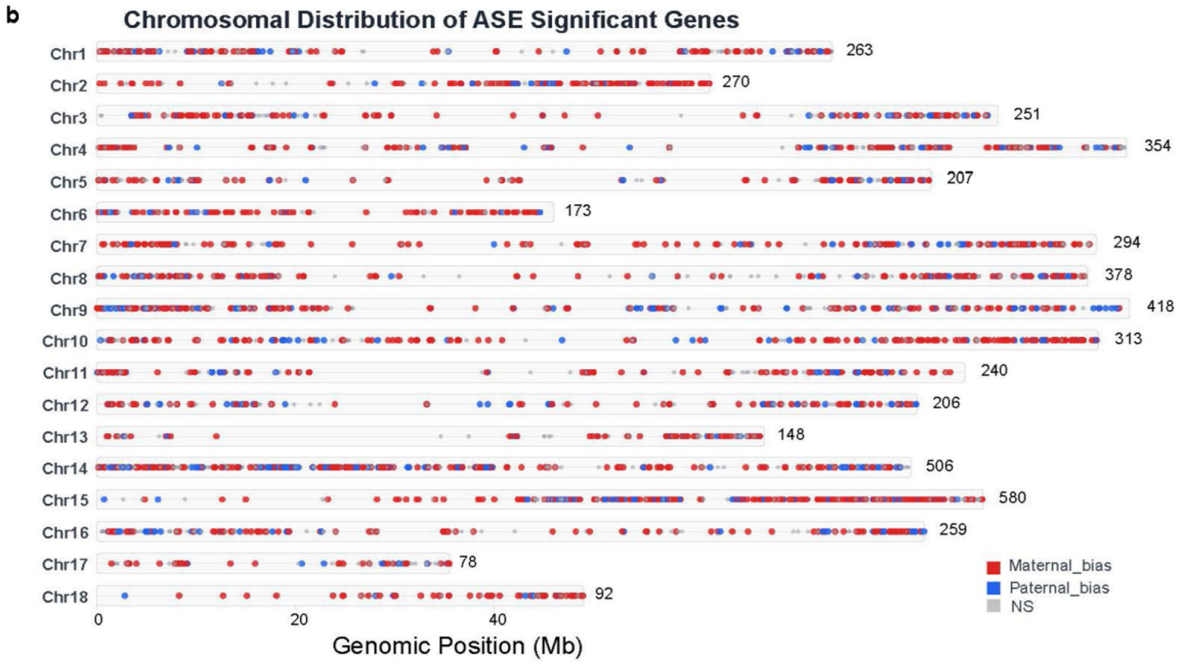


Figure 2. Genome-wide landscape of ASE. (**a**) Chromosomal distribution of phasing SNPs. (**b**) Chromosomal distribution of bias genes.

2.3. Monoallelic Expression and Extreme Allelic Bias

A total of 5030 genes exhibited allele-specific depth of at least 30 reads and a minimum of 2 informative SNPs per gene (Figure 3a,d, Supplementary Figures S2 and S3), representing approximately 11.84% of the reference rubber tree gene set. Among these, 2975 genes (59.2%) demonstrated significant allelic imbalance (FDR < 0.05, |allele reads fold change (aFC)| > 1). Maternal biased expression (aFC > 1) occurred in 2258 genes (44.9%), while paternal biased expression (aFC < −1) was observed in 717 genes (14.3%) (Figure 3b). The remaining 2055 genes (40.9%) were significant at FDR < 0.05 but fell below the |aFC| > 1 effect-size threshold (aFC = log2[(mat + 1)/(pat + 1)]) and were treated as not significant (NS). The maternal-to-paternal bias gene ratio of 3.15:1 indicated a genome-wide dominance of maternal gene expression in the F1 hybrid. The overall mean maternal allelic reads ratio (mat ratio) across all 5030 genes was 0.606 (Figure 3c). Complete monoallelic expression, where one parental allele contributed zero reads across all informative SNPs, was observed in 218 genes (4.3% of ASE genes), including 144 maternal reads-only genes (2.9%) and 74 paternal reads-only genes (1.5%).

GO and KEGG enrichment analyses were conducted for four ASE-defined gene sets: maternal bias (2258 genes), paternal bias (717 genes), 144 maternal bias (complete maternal monoallelic), and 74 paternal bias (complete paternal monoallelic). The maternal bias gene set exhibited significant enrichment (padj < 0.05) in eight GO terms. The paternal bias gene set revealed four significant GO terms. The enrichment results were illustrated in the heatmap presented in Figure 3e and Supplementary Figure S4.

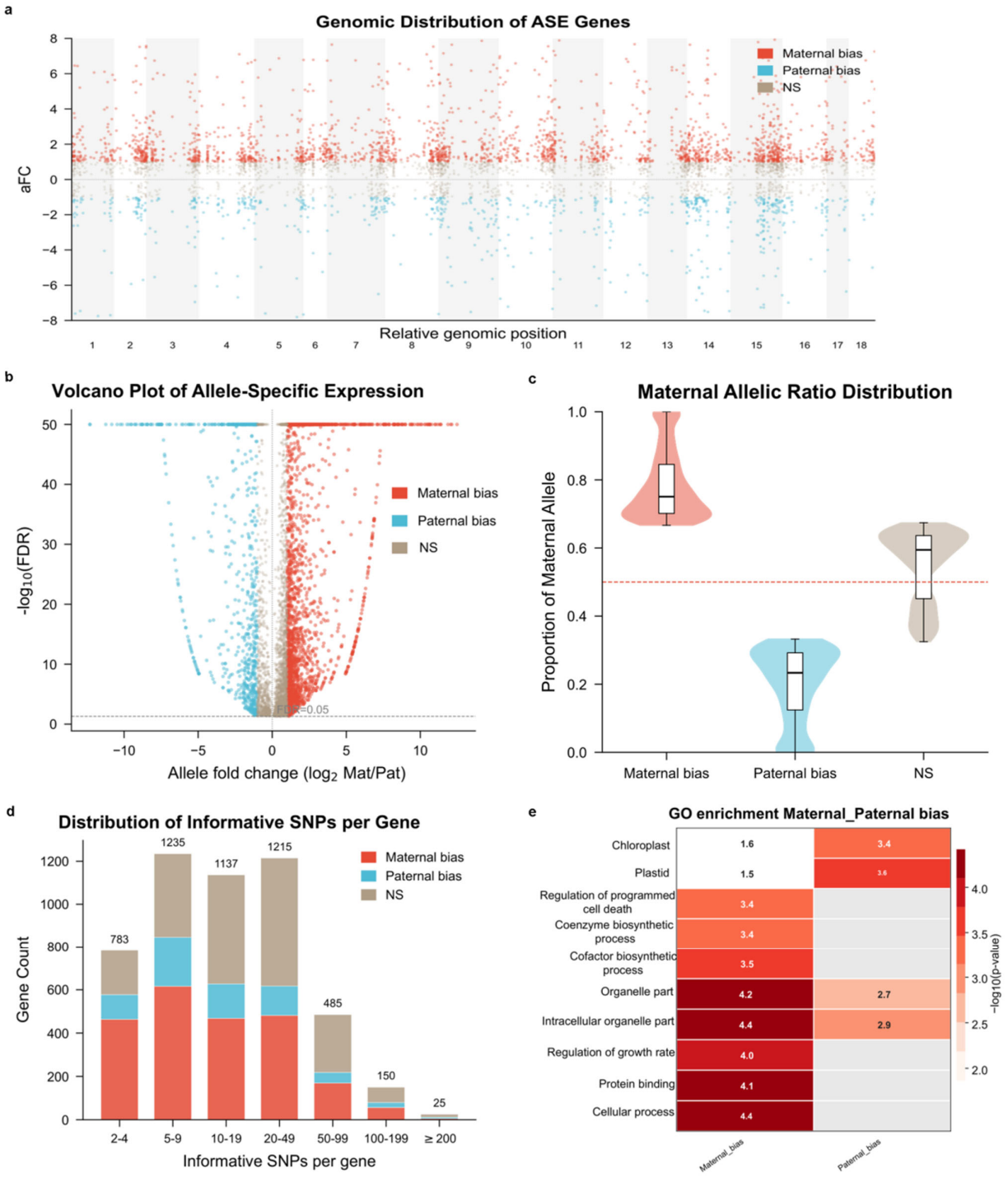


Figure 3. Allele-expression bias genes in triploid rubber tree. (**a**) Significant bias genes distributed. (**b**) Volcano plot of bias genes. (**c**) Allelic ratio of bias genes. (**d**) SNP number of bias genes. (**e**) GO enrichment of bias genes.

2.4. Temporal Expression Patterns of ASE Genes: Time Course Clustering with Low-Temperature Treatment

To characterize the temporal expression patterns of ASE genes following low-temperature treatment, we subjected maternal and paternal biased genes to fuzzy c-means clustering based on their z-score-normalized FPKM profiles across four time points (T0,

T2, T6, T20). After filtering for low expression and high variance, we retained 1994 maternal biased genes and 610 paternal biased genes for clustering.

For maternal-biased clusters (Figure 4a, Supplementary Figure S5), Cluster 1 (282 genes, 14.1%) exhibited a rapid response in T2 following low-temperature treatment and was enriched in histone modification and demethylase activity. Cluster 2 (487 genes, 24.4%) demonstrated a significant decrease in response to low-temperature treatment, with enrichment in chloroplast, plastid, and membrane-bound organelle functions. Cluster 3 (587 genes, 29.4%), the largest maternal cluster, showed a decrease in T2 with low-temperature treatment, with enrichment in protein binding, RNA binding, and ligase activity. Cluster 4 (329 genes, 16.5%) showed a significant increase in T2 following low-temperature treatment and was enriched in cellular processes, acyltransferase activity, and kinase binding. Cluster 5 (309 genes, 15.5%) exhibited an increase in T6 following low-temperature treatment, with enrichment in vacuolar membrane, cytosol, and cytoskeletal components.

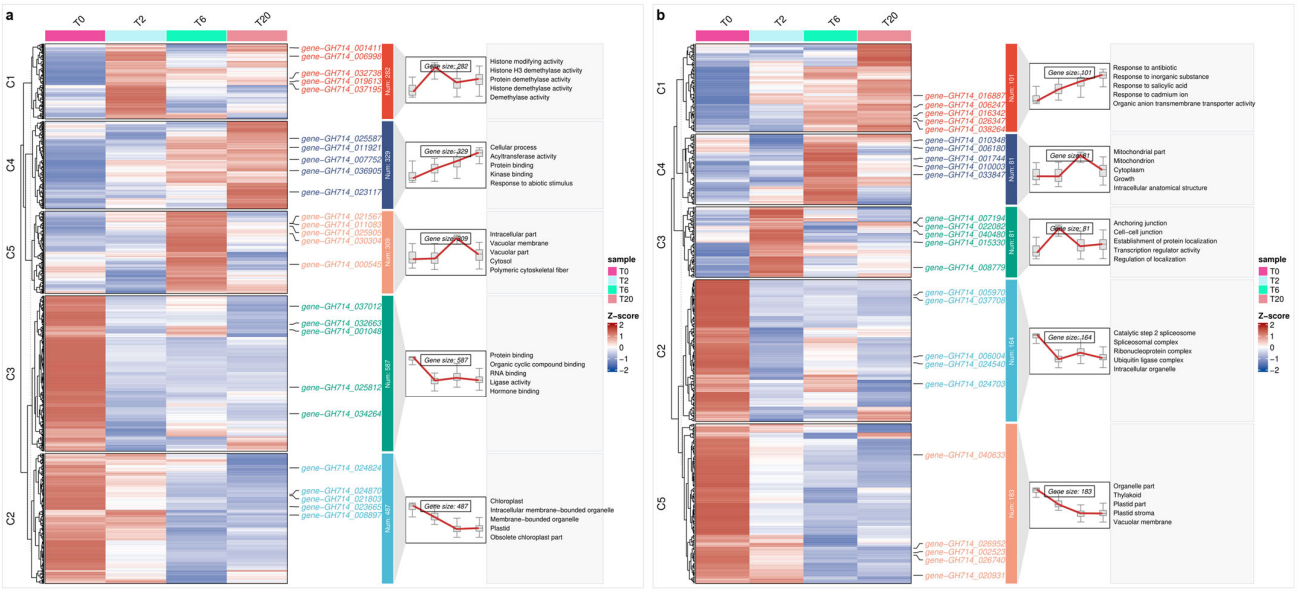


Figure 4. Clustering analysis bias genes with low-temperature treatment. (**a**) Clustering analysis of maternal-biased genes. (**b**) Clustering analysis of paternal-biased genes.

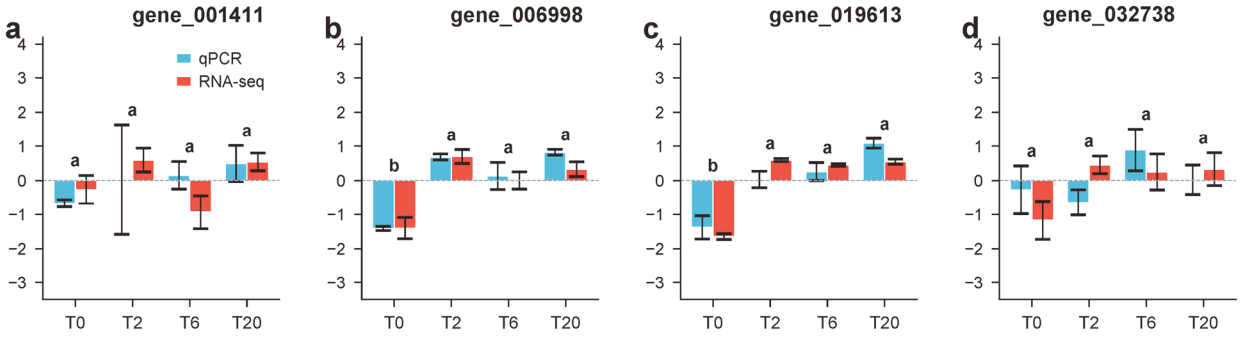
For paternal biased clusters (Figure 4b, Supplementary Figure S5), Cluster 1 (101 genes, 16.6%) exhibited a significant increase in low-temperature treatment and was enriched in antibiotic response, salicylic acid signaling, and cadmium ion response. Cluster 2 (164 genes, 26.9%) demonstrated a decrease at T2 in low-temperature treatment, with enrichment in catalytic step 2 spliceosome, spliceosomal complex, and ribonucleoprotein complex. Cluster 3 (81 genes, 13.3%) displayed a rapid response at T2 in low-temperature treatment and was enriched in cell–cell junctions, establishment of protein localization, and transcription regulator activity. Cluster 4 (81 genes, 13.3%) was characterized by an increase at T6 in low-temperature treatment, with enrichment in mitochondria and cytoplasm. Cluster 5 (183 genes, 30.0%), the largest paternal cluster, showed a significant decrease in low-temperature treatment and was enriched in thylakoid, plastid stroma, and vacuolar membrane.

2.5. Functional Enrichment of Biased Gene Sets and Expression Quantity Verification

Through enrichment analysis of ASE gene sets and trend analysis of low-temperature stress, we found that maternal-biased cluster 2 and paternal-biased cluster 5 exhibited a

significant reduction following low-temperature treatment, with enrichment in functions related to chloroplasts, plastids, and membrane-bound organelles. This finding indicated that low temperatures diminished plastid activity in rubber tree leaves, thereby impacting the growth of the rubber tree. Maternal-biased cluster 1 and paternal-biased cluster 3 demonstrated a rapid response in T2 after low-temperature treatment; however, the maternal-biased cluster was enriched in histone modification and demethylase activity, which regulated rapid gene responses at the epigenetic level. In contrast, the paternal-biased cluster was enriched in cell-to-cell junctions, protein localization, and transcription regulator activity, which governed cell communication and transcriptional regulation. The similar expression patterns observed in these two gene sets suggested a shared regulatory mechanism that governed the rapid response of rubber trees to low-temperature stress.

Ten key genes were selected for experimental validation through quantitative real-time PCR. Five genes were chosen from maternal cluster 1 (genes 037195, 032738, 019613, 006998, 001411, which encoded Zinc finger CCCH, GAPDH family, ubiquitin, DCD domain, and HEMB proteins) and five from paternal cluster 3 (genes 022082, 007194, 015330, 040480, 008779, which encoded cytochrome P450, BTB/POZ domain, MRS2–11, PLATZ, and WRKY). Primer pairs were designed using Primer3 (v2.6.1) based on the CDS sequences, and the primer sequences were provided in Supplementary Table S3. The quantitative real-time PCR results were calculated using the $2^{-\Delta\Delta Ct}$ method and visualized in Figure 5. Overall, the expression profiles obtained by qRT-PCR were moderately consistent with those generated by RNA-seq. Ten key genes were chosen from maternal cluster 1 and paternal cluster 3, which exhibited similar developmental expression trends across clusters, although slight differences in expression magnitude were observed for some genes. Pearson correlation analysis further demonstrated a significant positive correlation between the RNA-seq and qRT-PCR datasets ($r = 0.555$, $p < 0.001$), indicating a high level of agreement between the two methods. These results confirm the reliability of the transcriptome sequencing data and support the validity of the RNA-seq expressions to ASEG trends on which the clustered the ASEG set.



https://doi.org/10.3390/ijms272310751

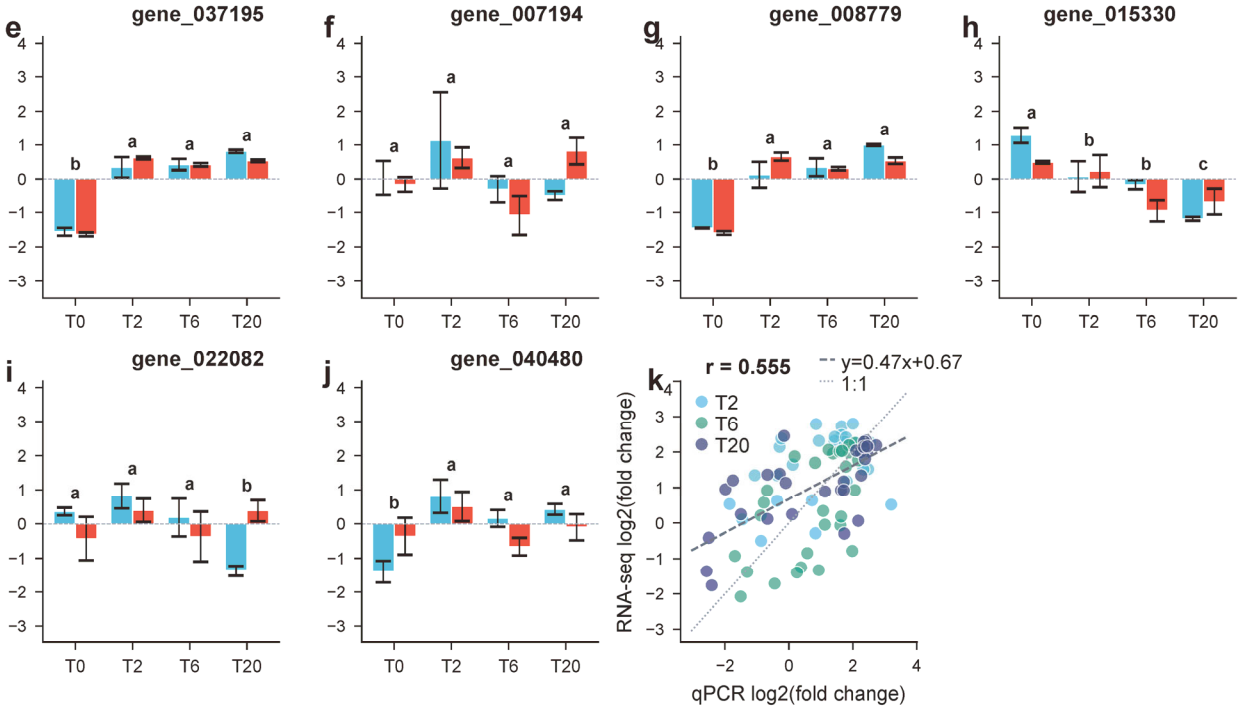


Figure 5. Validation of RNA-seq expression profiles of 10 representative genes. (**a**–**e**) Five genes from maternal cluster 1 (ma_C1): (**a**) HEMB (porphobilinogen synthase, gene_001411), (**b**) DCD domain (gene_006998), (**c**) ubiquitin (gene_019613), (**d**) GAPDH family (gene_032738), and (**e**) zinc finger CCCH (gene_037195). (**f**–**j**) Five genes from paternal cluster 3 (pa_C3): (f) BTB/POZ domain (gene_007194), (**g**) WRKY transcription factor (gene_008779), (**h**) Mg transporter MRS2-11 (gene_015330), (**i**) cytochrome P450 (gene_022082), and (**j**) PLATZ transcription factor (gene_040480). For each gene, expression levels were measured by qRT-PCR (blue) and RNA-seq (red) at four time points (T0, T2, T6, T20) with three biological replicates. All 10 genes displayed a rapid up-regulation peaking at T2 (2 h after cold treatment) followed by a decline, consistent with the expression trends of their respective clusters. (**k**) Correlation between RNA-seq (log2 fold change) and qRT-PCR (log2 relative expression) across the 10 genes (Pearson r = 0.555, $p < 0.001$).

3. Discussion

3.1. ASE Served as a Molecular Ruler for Heterosis in the Rubber Tree

ASE is arguably the most direct molecular readout of regulatory divergence between parental genomes inside an F1 hybrid. In 'Yunyan 77–4' we found 2975 genes with significant allelic imbalance, with maternal alleles contributing at a 3.15:1 ratio over paternal alleles. A caveat attaches to this headline number. Because the 'GT1' genome served as the reference, reads carrying maternal alleles match the reference more readily than paternal reads [11,36], so the observed ratio will tend to overshoot the true maternal contribution. In a triploid, the expected maternal:paternal genomic ratio is 2:1, and the deviation from that baseline is informative even though its exact size is uncertain. What makes us confident that a real maternal excess exists is the independent, sequence-level evidence: 144 genes are expressed exclusively from the maternal allele and 74 exclusively from the paternal allele, a 1.95:1 ratio (144 vs. 74), which approaches the 2:1 genomic dosage expectation. The scale of maternal dominance in rubber aligns with patterns in other perennials; for instance, tea plant F1 hybrids [12] displayed a similarly widespread maternal expression bias. The pervasiveness of ASE in the rubber tree indicated that cis-regulatory diver-

gence between the 'GT1' and 'PR107' genomes was not the exception but the norm. Furthermore, transcriptional complementation, where the two parental alleles contributed differentially to the hybrid transcriptome, represented a fundamental feature of rubber tree heterosis. Besides, a particularly striking result involved the identification of 218 completely monoallelically expressed genes. Their proportion is markedly higher than the figures reported for annual crops such as maize and rice, which is consistent with the long generation time and predominantly outcrossing history of rubber, both of which should allow cis-regulatory divergence to accumulate between parental haplotypes. These monoallelic genes represented prime candidates for testing the dominance model of heterosis, wherein the functional allele from one parent compensated for a defective or silenced allele from the other. If these genes mapped to quantitative trait loci (QTL) associated with latex yield, disease resistance, or stress tolerance, they directly linked molecular ASE to agronomic heterosis.

The GO functional enrichment patterns supported a scenario of functional complementation between the parental genomes. Maternal-biased genes were enriched in housekeeping and biosynthetic processes, including chloroplast function, protein modification (histone demethylation, ubiquitination), and primary metabolism (GAPDH, ubiquitin). In contrast, paternal-biased genes exhibited enrichment in stress-responsive and regulatory pathways, such as antibiotic response, salicylic acid signaling, and transcription factor activity (WRKY, PLATZ). This division of labor, with the maternal genome driving core metabolism and the paternal genome contributing to stress adaptation, mirrored a pattern observed in rice hybrids [7] and represented a conserved strategy for hybrid vigor across plant species, where one parent provided metabolic robustness while the other conferred environmental responsiveness.

3.2. Methodological Strengths of the Present ASE Pipeline

The reliability of ASE calls depended critically on the quality of each upstream step, from variant discovery to statistical inference. Our pipeline incorporated three design features that collectively strengthened the confidence and interpretability of the results. Trio-based joint genotyping and stringent filtering explicitly informed every genotype call through the trio relationship, while a depth-based blacklist removed low-confidence and repetitive loci prior to phasing. The informative SNP definition, which required F1 heterozygosity with reciprocal parental homozygosity, ensured unambiguous parent of origin assignment for every allele-specific read. This criterion was stricter than the commonly used F1 heterozygous filter and eliminated approximately 25% of heterozygous sites where both parents shared one allele, which could confound ASE attribution. We aligned F1 RNA-seq reads using STAR in WASP mode and retained only reads tagged vW:i:1. WASP remapped each read with both alleles forced at every SNP and discarded reads whose alignment positions changed, thereby removing the systematic bias that caused reference matching reads to map preferentially. WASP is currently the gold standard for this correction [24,25,36], although some residual bias cannot be excluded. A gene-level ASE test aggregates counts across multiple SNPs within the same transcriptional unit. Aggregating reads over all informative SNPs within a gene and testing with a beta-binomial likelihood-ratio model yields conservative, biologically meaningful ASE calls, because overdispersion across SNPs is explicitly accommodated rather than ignored.

3.3. Toward a Multi-Omic Dissection of Hybrid Vigour Through ASE

This study provided a genome-wide, time-resolved ASE map for rubber tree and established an analytical framework that linked ASV to ASE. This framework offered a practical analytical approach for investigating hybrid vigor in triploid rubber trees.

Our analysis focused on a single F1 genotype ('Yunyan 77–4') and a specific tissue type (leaf) over a time course. ASE varied significantly across genotypes [37,38] and tissues [7]. Expanding the study to include other hybrid genotypes, particularly those with well characterized heterosis phenotypes for latex yield, girth, or disease resistance, enabled quantitative mapping of genotype to ASE to phenotype associations. Furthermore, profiling ASE in latex, bark, root, and other tissues captured the spatial dimension of allelic imbalance, which was especially relevant for rubber trees due to the tissue specificity of natural rubber biosynthesis [39]. Parental differences in DNA methylation, particularly at CHG and CHH contexts, were causally linked to ASE in hybrid rice [15]. Whole-genome bisulfite sequencing (WGBS) of the F1 hybrid and both parents identified differentially methylated regions (DMRs) between parental alleles and tested whether allele-specific methylation at promoters or gene bodies correlated with the magnitude and direction of ASE. They demonstrated that hybrids of the tea plant [12] exhibited more accessible chromatin regions compared to their parental lines, and that allele-specific chromatin accessibility correlated with ASE. Future ATAC-seq analysis of rubber tree hybrid tissues could reveal whether maternal-biased genes associate with maternal-specific open chromatin. Furthermore, specific families of transcription factors, identified through motif enrichment in allele-specific accessible chromatin regions (ACRs), mediated the allelic imbalance. Bulk RNA-seq averaged expression across heterogeneous cell populations. In rubber tree latex, laticifers were the specialized cells responsible for rubber biosynthesis, coexisting with companion cells and parenchyma. The scRNA-seq of hybrid tissues resolved ASE to a cellular resolution.

In our study, we established an ASV-to-ASE analysis workflow for triploid rubber trees and utilized ASE analysis to elucidate hybrid vigor. However, our investigation remained confined to a single triploid variety and tissue type. We did not examine aspects of epigenetic regulation, such as methylation and open chromatin, and thus could not fully explain the hybrid vigor of triploid rubber trees. Nevertheless, the analytical pipeline we proposed served as a foundation for studying tissue-specific and variety-specific expression of ASE in triploid rubber trees, thereby clarifying the mechanisms that regulated cold tolerance and hybrid vigor in rubber trees.

4. Materials and Methods

4.1. Plant Material and Experimental Design

We studied ASE in the rubber tree using one-year-old budded plantlets from the rubber tree clone 'Yunyan 77–4', a triploid F1 hybrid ($3n = 54$) derived from a cross between the maternal parent 'GT1' ($2n = 36$) and the paternal parent 'PR107' ($2n = 36$). The plantlets grew in the nursery of the National Germplasm Repository of Rubber Tree in Jinghong City, under the Ministry of Agriculture, located in the Yunnan Institute of Tropical Crops (YITC), Jinghong, Yunnan, China (22°0′ N, 100°46′ E). Leaf material from the F1 was collected at four time points (0 h, 2 h, 6 h, 20 h) and exposed to continuous 4 °C treatment, which included an 8 h/16 h dark/light cycle, a light intensity of 10,000 lx, and 75% relative humidity, with three biological replicates each. The leaf samples were frozen in liquid nitrogen immediately after collection and stored in an ultra-low temperature freezer at -80 °C. Total RNA was extracted from all samples using TRIzol reagent (Invitrogen, Carlsbad, CA, USA), followed by library construction, and sequencing was performed as 150 bp paired-end reads on an Illumina NovaSeq6000 platform (Illumina, San Diego, CA, USA); sequencing performed by Biomarker Technologies Co., Ltd. (Beijing, China). For qRT-PCR validation, first-strand cDNA synthesis utilized the TransScript gDNA Removal and cDNA Synthesis SuperMix (TransGen Biotech, Beijing, China), and quantitative PCR was conducted with SYBR Premix ExTaq (Takara Bio, Kusatsu, Shiga, Japan) on the Ana-

lytik Jena qTOWER 2.2 real-time PCR detection system (Analytik Jena AG, Jena, Germany). Relative expression levels were calculated with the $2^{-\Delta\Delta Ct}$ method [40], using *Hbβ-actin* as the internal reference; primer sequences are listed in Supplementary Table S3. The resequencing data for the two parents and the F1 were downloaded from the National Genomics Data Center (https://ngdc.cncb.ac.cn/) using the sample IDs provided in the publications (Supplementary Table S1), which allowed variants to be assigned to their parental origin.

4.2. Variant Calling and Phasing

The published reference genome of *H. brasiliensis* (GT1) [41] and its gene annotation were used for both DNA and RNA mapping. Indexes were prepared as follows: a FASTA index with samtools (v1.21) faidx [42], a sequence dictionary with GATK4 (v.4.5.0.0) CreateSequenceDictionary [43], a BWA index with bwa-mem2 (v2.3) index [44], and a STAR (v2.7.11b) genome index with STAR --runMode genomeGenerate [45]. Resequencing reads were aligned to the reference genome using bwa-mem2 and sorted with samtools. Variants were called per sample in GVCF mode with GATK4 HaplotypeCaller with ploidy = 2, and GVCFs were combined using CombineGVCFs and jointly genotyped with GenotypeGVCFs, allowing the trio relationship to inform each genotype. Hard filters were then applied to remove sites with QD < 2.0, FS > 60.0, or MQ < 40.0, thereby retaining only biallelic SNPs. Before phasing, a coverage blacklist was constructed from the BAM files; samtools idxstats estimated the mean sequencing depth, bedtools (v2.31.1) [46] genomecov measured per-base coverage, and any region with coverage below 3× the mean or above 5× the mean was flagged. Flagged intervals were merged into a blacklist using bedtools merge. To assign each heterozygous F1 site to its parental source, phased the variants using whatshap (v2.8) [47], which utilized read-level haplotype information within each sample [48], then merged the data across samples with bcftools (v1.25) [49]. The resulting phased VCF indicated that for each heterozygous variant, the allele SNP site exhibited 0/1 phasing as 1|0 or 0|1. These sites were extracted with a cyvcf2 (v0.34) [50] based script, and discarded any site overlapping the depth blacklist. The variants were designated such that the allele from 'PR107' represented the paternal allele, while the allele from 'GT1' represented the maternal allele.

4.3. Allele-Specific Expression Analysis

F1 RNA-seq reads were aligned with STAR in WASP mode, which provided the informative SNPs through the --varVCFfile option and set the --waspOutputMode to SAMtag. WASP remapped each read twice, once with the reference allele enforced at the SNP and once with the alternate allele. It retained the read only if both mappings agreed on its location. Reads that passed the WASP filtering were tagged as vW:i:1 in the BAM file. The alignment was then filtered to retain only these reads and indexed using samtools. For each biological replicate, allele-specific reads overlapping every informative SNP were counted with GATK4 ASEReadCounter, requiring a minimum mapping quality of 20 and a minimum base quality of 20. The three replicate count tables were merged, and within each gene, the maternal and paternal read counts across all informative SNPs were summed. Gene identity was established by intersecting SNP coordinates with exon locations derived from gene annotation using bedtools (v2.31.1) [46]. A gene was carried forward only if its total allele-specific depth reached at least 30 reads and was supported by a minimum of two informative SNPs, specifically, total depth ≥ 30 and n-snps ≥ 2. These cut-offs protected against genes where a single SNP or a limited number of low-coverage reads could dominate the estimate. Each gene was modeled using a beta-binomial likelihood-ratio test (a two-step procedure: initial screening with a binomial test under the null hypothesis $p = 0.5$ with FDR correction, followed by classification using the reads fold

effect-size threshold |aFC| > 1), where the test statistic represented twice the difference in log-likelihood, compared to a χ^2 distribution with one degree of freedom. *p*-Values were corrected across all tested genes using the Benjamini–Hochberg procedure (FDR). Each gene was summarized by its allelic fold change, aFC = log2((mat + 1)/(pat + 1)), and its maternal ratio, mat_ratio = mat/(mat + pat). Genes with FDR < 0.05 and aFC > 1, indicating maternal reads exceeded paternal reads by more than twice, with mat_ratio > 0.667, were classified as having maternal bias. Conversely, those with FDR < 0.05 and aFC < −1, where paternal reads surpassed maternal reads by more than twice, with mat_ratio < 0.333, were classified as having paternal bias; the remaining genes were considered not significant for allelic imbalance.

4.4. Biased Genes Function Analysis

To examine how allelic bias changed with low-temperature treatment, we focused on the maternal and paternal biased gene sets separately. Time-course FPKM values at T0, T2, T6, and T20 (three replicates per time point) were retrieved for each gene. We averaged the replicate values at each time point and removed genes with a mean FPKM below 1 or a standard deviation below 0.5 across the time course, as these were deemed uninformative. The remaining expression profiles were z-scored per gene and clustered using fuzzy c-means via Mfuzz (v2.70) [51], with a fuzzifier of m = 2, k = 5, and random seed 42 for reproducibility. Each gene was assigned to the cluster with the highest membership. We ordered the clusters by their peak time point to enhance the readability of temporal patterns. We assigned protein functions using eggNOG-mapper (v2.1.13) [52], which provided each gene with GO terms and KEGG orthology annotations. We constructed a database with AnnotationForge (https://github.com/Bioconductor/AnnotationForge, accessed on 27 July 2026) based on the eggNOG annotations, encompassing 40,800 genes with GO/KO mappings. We performed GO and KEGG enrichment analyses for each gene set using clusterProfiler (v4.18.4) [53], applying the hypergeometric test with BH adjustment for significance. We tested the ASE-defined sets, maternal bias, and paternal bias, alongside the ten time course clusters. We visualized the enriched terms as bubble plots and heatmaps using ggplot2 [54].

5. Conclusions

In this study, we established a cold tolerance time-resolved map of ASE for *Hevea brasiliensis*, utilizing the F1 hybrid 'Yunyan 77–4' and its parental clones 'GT1' and 'PR107', along with their whole genome sequencing (WGS) reads and F1 RNA sequencing (RNA-seq) reads. Our analysis revealed a principal finding regarding the F1 hybrid transcriptome, characterized by a significant genome-wide maternal bias genes expression dominance, with a maternal bias genes to paternal ratio of 3.15:1 and a mean maternal allelic reads ratio of 0.606. We identified 218 completely monoallelic genes, comprising 144 expressed solely from the maternal allele and 74 from the paternal allele, yielding a ratio of 2:1. Allele-specific expression genes (ASEGs) were functionally partitioned between the parental genomes. Clustering analysis grouped maternal-biased genes into distinct patterns, which were dominated by housekeeping and biosynthetic functions, chloroplast biogenesis, histone modification, and protein/RNA binding. In contrast, paternal-biased genes formed clusters enriched in stress-responsive and regulatory pathways, including antibiotic and salicylic acid signaling, spliceosome assembly, and transcription factor activity. This division of labor indicated that the maternal genome supported core metabolism, while the paternal genome enhanced environmental responsiveness. This complementary interaction between the two parental genomes provided a functional-enrichment-based hypothesis for hybrid vigor, supposing that they jointly expanded the hybrid's physiological repertoire throughout the entire growth cycle. The methodological

framework developed included phase joint genotyping, WASP-corrected read mapping, and beta-binomial overdispersion modeling, which provided a reproducible and generalizable template for ASE analysis in triploid rubber trees. Collectively, these results positioned ASE as a tractable molecular phenotype for dissecting heterosis in triploid rubber trees. Looking forward, the integration of ASE with whole-genome bisulfite sequencing (WGBS), ATAC-seq, and scRNA-seq aimed to enhance the understanding of how parental genomes interacted in the hybrid to produce the emergent property of hybrid vigor, which carried direct implications for molecular breeding and genome editing strategies focused on improving latex yield.

Supplementary Materials: The following supporting information can be downloaded at: https://www.mdpi.com/article/10.3390/ijms272310751/s1.

Author Contributions: C.Z. contributed to the conceptualization and design of the study, development and implementation of the methodology, formal data analysis, figure preparation and visualization, preparation of the original draft, and review and editing of the manuscript. C.L. and J.Z. provided experimental materials, equipment, and other resources. Y.N. and C.M. were responsible for supervision, project administration, and coordination. J.L. was responsible for funding acquisition. All authors have read and agreed to the published version of the manuscript.

Funding: This work was supported by Project of Yunnan Provincial Basic Research Program (No. 202601AS070002, No. 202401AS070083), the Joint Project of Agricultural Basic Research of Yunnan Province (No. 202601BD070001–121), Yunnan Technology Innovation Center of Natural Rubber (No. 202605AK340010), Yunnan Key Laboratory of Sustainable Utilization Research on Rubber Tree (No. 202605AV340001), Yunnan Academician & Expert Workstation Project (No. 202605AF350029), the Scitech Innovation System Construction for Tropical Crops Grant of Yunnan Province (No. RF2026) and Funding for QNCZ of YITC (No. QNCZ2026–4).

Institutional Review Board Statement: Not applicable.

Informed Consent Statement: Not applicable.

Data Availability Statement: The whole-genome resequencing reads and RNA-seq data supporting this study have been deposited in a public data repository; accessions are listed in Supplementary Table S1.

Conflicts of Interest: The authors declare no conflicts of interest.

Abbreviations

The following abbreviations are used in this manuscript:

ACR	Accessible Chromatin Region
ASE	Allele-specific expression
ASEG	Allele-specific expression genes
ASV	Allele-specific variants
ATAC-seq	Assay for Transposase-Accessible Chromatin using sequencing
aFC	Allele reads fold change
DMR	Differentially Methylated Region
FDR	False Discovery Rate
FPKM	Fragments Per Kilobase of transcript per Million mapped reads
GO	Gene Ontology
KEGG	Kyoto Encyclopedia of Genes and Genomes
qRT-PCR	quantitative Real-Time PCR
QTL	Quantitative Trait Locus
RNA-seq	RNA sequencing
scRNA-seq	single-cell RNA sequencing

SDR	Meiosis second-division restitution
SNP	Single Nucleotide Polymorphism
T2T	Telomere-to-Telomere
WGBS	Whole-Genome Bisulfite Sequencing
WGS	Whole-Genome Sequencing

References

1. Li, Z.; Zhao, Y.; Luo, K. Molecular Mechanisms of Heterosis and Its Applications in Tree Breeding: Progress and Perspectives. *Int. J. Mol. Sci.* **2024**, *25*, 12344. https://doi.org/10.3390/ijms252212344.
2. Wittkopp, P.J.; Haerum, B.K.; Clark, A.G. Evolutionary changes in cis and trans gene regulation. *Nature* **2004**, *430*, 85–88. https://doi.org/10.1038/nature02698.
3. Botet, R.; Keurentjes, J.J.B. The Role of Transcriptional Regulation in Hybrid Vigor. *Front. Plant Sci.* **2020**, *11*, 410. https://doi.org/10.3389/fpls.2020.00410.
4. St. Pierre, C.L.; Macias-Velasco, J.F.; Wayhart, J.P.; Yin, L.; Semenkovich, C.F.; Lawson, H.A. Genetic, epigenetic, and environmental mechanisms govern allele-specific gene expression. *Genome Res.* **2022**, *32*, 1042–1057. https://doi.org/10.1101/gr.276193.121.
5. Dai, H.; Bai, X.; Wang, J.; Chai, Y.; Fu, S.; Liu, Y. Research Progress on Formation Mechanism of Allele Specific Expression and Its Application. *Anim. Husb. Feed. Sci.* **2019**, *40*, 37–40. https://doi.org/10.16003/j.cnki.issn1672-5190.2019.06.011.
6. Mattevi, S.; Mazzarotto, F.; Martini, P. Allele-specific expression analysis: Pipelines, applications, challenges, and unmet needs. *Comput. Biol. Med.* **2025**, *196*, 110890. https://doi.org/10.1016/j.compbiomed.2025.110890.
7. Shao, L.; Xing, F.; Xu, C.; Zhang, Q.; Che, J.; Wang, X.; Song, J.; Li, X.; Xiao, J.; Chen, L.L.; et al. Patterns of genome-wide allele-specific expression in hybrid rice and the implications on the genetic basis of heterosis. *Proc. Natl. Acad. Sci. USA* **2019**, *116*, 5653–5658. https://doi.org/10.1073/pnas.1820513116.
8. Li, D.; Lu, X.; Zhu, Y.; Pan, J.; Zhou, S.; Zhang, X.; Zhu, G.; Shang, Y.; Huang, S.; Zhang, C. The multi-omics basis of potato heterosis. *J. Integr. Plant Biol.* **2022**, *64*, 671–687. https://doi.org/10.1111/jipb.13211.
9. Gao, W.; Wang, S.; Jiang, T.; Hu, H.; Gao, R.; Zhou, M.; Wang, G. Chromosome-scale and haplotype-resolved genome assembly of Populus trichocarpa. *Hortic. Res.* **2025**, *12*, uhaf012. https://doi.org/10.1093/hr/uhaf012.
10. Lei, W.; Zhang, Y.; Wang, Y.; Yu, J.; Li, H.; Hou, X.; Fan, W.; Xiao, Y.; Yan, J.; Lei, X.; et al. Haplotype-resolved genome reveals allele-aware epigenetic and 3D chromatin regulation of heterosis in the tea hybrid. *New Phytol.* **2026**, *250*, 404–421. https://doi.org/10.1111/nph.70908.
11. Stevenson, K.R.; Coolon, J.D.; Wittkopp, P.J. Sources of bias in measures of allele-specific expression derived from RNA-seq data aligned to a single reference genome. *BMC Genom.* **2013**, *14*, 536. https://doi.org/10.1186/1471-2164-14-536.
12. Wang, P.; Gu, M.; Yu, X.; Shao, S.; Du, J.; Wang, Y.; Wang, F.; Chen, S.; Liao, Z.; Ye, N.; et al. Allele-specific expression and chromatin accessibility contribute to heterosis in tea plants (*Camellia sinensis*). *Plant J.* **2022**, *112*, 1194–1211. https://doi.org/10.1111/tpj.16004.
13. Zhou, H.; Deng, X.W.; He, H. Gene expression variations and allele-specific expression of two rice and their hybrid in caryopses at single-nucleus resolution. *Front. Plant Sci.* **2023**, *14*, 1171474. https://doi.org/10.3389/fpls.2023.1171474.
14. Shevtsov, A.; Buyan, A.; Nozdrin, V.; Akhtyamov, P.; Stupnikov, A.; Meshcheryakov, G.; Kulakovskiy, I.V.; Medvedeva, Y.A. NEXT-scASV: A Nextflow pipeline for allele-specific variant calling from single-cell RNA-seq data. *GigaScience* **2026**, *15*, giag042. https://doi.org/10.1093/gigascience/giag042.
15. Ma, X.; Xing, F.; Jia, Q.; Zhang, Q.; Hu, T.; Wu, B.; Shao, L.; Zhao, Y.; Zhang, Q.; Zhou, D.X. Parental variation in CHG methylation is associated with allelic-specific expression in elite hybrid rice. *Plant Physiol.* **2021**, *186*, 1025–1041. https://doi.org/10.1093/plphys/kiab088.
16. Springer, N.M.; Stupar, R.M. Allelic variation and heterosis in maize: How do two halves make more than a whole? *Genome Res.* **2007**, *17*, 264–275. https://doi.org/10.1101/gr.5347007.
17. Zhou, P.; Hirsch, C.N.; Briggs, S.P.; Springer, N.M. Dynamic Patterns of Gene Expression Additivity and Regulatory Variation throughout Maize Development. *Mol. Plant* **2019**, *12*, 410–425. https://doi.org/10.1016/j.molp.2018.12.015.
18. Afzal, R. Identification of Allele-Specific Expression of Hybrid Maize and its Association with Heterosis. Master's Thesis, Huazhong Agricultural University, Wuhan, China, 2023. https://doi.org/10.27158/d.cnki.ghznu.2023.001664.

19. Pitz, M.; Baldauf, J.A.; Piepho, H.; Hochholdinger, F. Nonadditive gene expression contributing to heterosis in partially heterozygous maize hybrids is predominantly regulated from heterozygous regions. *New Phytol.* **2025**, *247*, 669–683. https://doi.org/10.1111/nph.70128.
20. Liu, X.; Li, Y.; Li, C.; Zhang, D.; He, G.; Liu, H.; Sun, S.; Li, Y.; Guo, M.; Wang, T. Dynamics of Gene and Allelic Expression During Modern Hybrid Maize Breeding. *Plant Biotechnol. J.* **2026**, *24*, 3922–3938. https://doi.org/10.1111/pbi.70602.
21. Gao, Z.; Li, H.; Yang, X.; Yang, P.; Chen, J.; Shi, T. Biased allelic expression in tissues of F1 hybrids between tropical and temperate lotus (*Nelumbo nucifera*). *Plant Mol. Biol.* **2021**, *106*, 207–220. https://doi.org/10.1007/s11103-021-01138-8.
22. Wu, X.; Chen, X.; Wang, R.; Wang, H.; Hu, X.; Wang, Y.; Li, G.; Dong, N.; Hu, T.; Ru, Z. Transcriptome dynamics and allele-specific regulation underlie wheat heterosis at the anthesis and grain-filling stages. *BMC Genom.* **2025**, *26*, 798. https://doi.org/10.1186/s12864-025-11983-2.
23. Bell, G.D.; Kane, N.C.; Rieseberg, L.H.; Adams, K.L. RNA-Seq Analysis of Allele-Specific Expression, Hybrid Effects, and Regulatory Divergence in Hybrids Compared with Their Parents from Natural Populations. *Genome Biol. Evol.* **2013**, *5*, 1309–1323. https://doi.org/10.1093/gbe/evt072.
24. van de Geijn, B.; McVicker, G.; Gilad, Y.; Pritchard, J.K. WASP: Allele-specific software for robust molecular quantitative trait locus discovery. *Nat. Methods* **2015**, *12*, 1061–1063. https://doi.org/10.1038/nmeth.3582.
25. Asiimwe, R.; Alexander, D. STAR+WASP reduces reference bias in the allele-specific mapping of RNA-seq reads. *bioRxiv* **2024**. https://doi.org/10.1101/2024.01.21.576391.
26. Tang, C. Research Progress on Biology of Rubber Production in Rubber Tree. *Chin. J. Trop. Crop.* **2020**, *41*, 1958–1967. https://doi.org/10.3969/j.issn.1000-2561.2020.10.003.
27. Li, L.; Gui, M.; Guan, Y.; Mao, C.; Tian, H.; Zhang, F. Cold Resistance of Rubber Trees (*Hevea brasiliensis*) by Combined Recovery and Conductivity Analysis. *Chin. J. Trop. Crop.* **2021**, *42*, 370–377. https://doi.org/10.3969/j.issn.1000-2561.2021.02.011.
28. Li, X.; Zhang, F.; Wu, Y.; Mao, C.; Yang, T. Comparison of Cold Tolerance of 42 Hevea brasiliensis Germplasm Resources. *Trop. Agric. Sci. Technol.* **2023**, *46*, 49–53. https://doi.org/10.16005/j.cnki.tast.2023.03.009.
29. Mao, C.; Li, L.; Yang, T.; Gui, M.; Li, X.; Zhang, F.; Zhao, Q.; Wu, Y. Transcriptomics integrated with widely targeted metabolomics reveals the cold resistance mechanism in Hevea brasiliensis. *Front. Plant Sci.* **2023**, *13*, 1092411. https://doi.org/10.3389/fpls.2022.1092411.
30. Ao, S.; He, L.; Xiao, G.; Chen, J.; He, C. Selection of Rubber Cold Fast and High-Yield Strains, Yunyan 77-2 and Yunyan 77-4. *Yunnan Trop. Crop. Sci. Technol.* **1998**, *2*, 4–9. https://doi.org/10.16005/j.cnki.tast.1998.02.001.
31. Li, H.; Zhou, T.; Ning, L.; Li, G. Cytological Identification and Breeding Course of Hevea 'Yunyan 77-2' and 'Yunyan 77-4'. *J. Trop. Subtrop. Bot.* **2009**, *17*, 602–605. https://doi.org/10.3969/j.issn.1005-3395.2009.6.2323.
32. Ao, S.; He, L.; Xiao, G. Primary Report on Regional Planting High-yield, Resisting Cold Rubber Clone in Yunnan. *Yunnan Trop. Crop. Sci. Technol.* **2000**, *2*, 1–5. https://doi.org/10.16005/j.cnki.tast.2000.02.001.
33. Yao, P.; Li, G.; Long, Q.; He, L.; Kang, X. Male Parent Identification of Triploid Rubber Trees (*Hevea brasiliensis*) and the Mechanism of 2n Gametes Formation. *Forests* **2016**, *7*, 301. https://doi.org/10.3390/f7120301.
34. Zhang, Y.; Li, H.; Huang, X.; Yuan, Y.; Zhang, X.; Gao, X.; Wang, X.; Wei, M.; Huang, H.; Li, W. Heterozygosity analysis of spontaneous 2n female gametes and centromere mapping of the diploid Hevea brasiliensis based on full-sib triploid populations. *Plant Reprod.* **2024**, *37*, 47–56. https://doi.org/10.1007/s00497-023-00481-8.
35. Zhang, Y.; Zhang, X.; Huang, X.; Zhang, X.; Yao, P.; Li, W. Low-temperature increases the frequency of 2n female gametes in the diploid rubber tree (*Hevea brasiliensis* (Willd. ex A.Juss.) Müll. Arg.). *Tree Genet. Genomes* **2019**, *15*, 23. https://doi.org/10.1007/s11295-019-1330-0.
36. Degner, J.F.; Marioni, J.C.; Pai, A.A.; Pickrell, J.K.; Nkadori, E.; Gilad, Y.; Pritchard, J.K. Effect of read-mapping biases on detecting allele-specific expression from RNA-sequencing data. *Bioinformatics* **2009**, *25*, 3207–3212. https://doi.org/10.1093/bioinformatics/btp579.
37. Springer, N.M.; Stupar, R.M. Allele-Specific Expression Patterns Reveal Biases and Embryo-Specific Parent-of-Origin Effects in Hybrid Maize. *Plant Cell* **2007**, *19*, 2391–2402. https://doi.org/10.1105/tpc.107.052258.
38. Zhou, T.; Zhang, J.; Liang, Y.; Gu, R.; Ma, Y.; Zhu, W.; Li, J.; Du, X.; Wang, X.; Wang, P.; et al. Nonadditive regulation confers phenotypic variation in hybrid maize. *New Phytol.* **2025**, *246*, 631–644. https://doi.org/10.1111/nph.20453.
39. Li, C.; Yuan, Y.; Nie, Z.; Wu, T.; Wang, Z.; Qiao, J.; Deng, Z.; Wang, X.; Xu, D.; Wang, X.; et al. The haplotype-resolved telomere-to-telomere genome and OMICS analyses reveal genetic responses to tapping in rubber tree. *Nat. Commun.* **2025**, *16*, 6255. https://doi.org/10.1038/s41467-025-61527-1.

40. Livak, K.J.; Schmittgen, T.D. Analysis of Relative Gene Expression Data Using Real-Time Quantitative PCR and the $2^{-\Delta\Delta CT}$ Method. *Methods* **2001**, *25*, 402–408. https://doi.org/10.1006/meth.2001.1262.
41. Liu, J.; Shi, C.; Shi, C.C.; Li, W.; Zhang, Q.J.; Zhang, Y.; Li, K.; Lu, H.F.; Shi, C.; Zhu, S.T.; et al. The Chromosome-Based Rubber Tree Genome Provides New Insights into Spurge Genome Evolution and Rubber Biosynthesis. *Mol. Plant* **2020**, *13*, 336–350. https://doi.org/10.1016/j.molp.2019.10.017.
42. Li, H.; Handsaker, B.; Wysoker, A.; Fennell, T.; Ruan, J.; Homer, N.; Marth, G.; Abecasis, G.; Durbin, R. The Sequence Alignment/Map format and SAMtools. *Bioinformatics* **2009**, *25*, 2078–2079. https://doi.org/10.1093/bioinformatics/btp352.
43. DePristo, M.A.; Banks, E.; Poplin, R.; Garimella, K.V.; Maguire, J.R.; Hartl, C.; Philippakis, A.A.; del Angel, G.; Rivas, M.A.; Hanna, M.; et al. A framework for variation discovery and genotyping using next-generation DNA sequencing data. *Nat. Genet.* **2011**, *43*, 491–498. https://doi.org/10.1038/ng.806.
44. Li, H. Aligning Sequence Reads, Clone Sequences and Assembly Contigs with BWA-MEM. *arXiv* **2013**, arXiv:1303.3997. https://doi.org/10.48550/arXiv.1303.3997.
45. Dobin, A.; Davis, C.A.; Schlesinger, F.; Drenkow, J.; Zaleski, C.; Jha, S.; Batut, P.; Chaisson, M.; Gingeras, T.R. STAR: Ultrafast universal RNA-seq aligner. *Bioinformatics* **2013**, *29*, 15–21. https://doi.org/10.1093/bioinformatics/bts635.
46. Quinlan, A.R.; Hall, I.M. BEDTools: A flexible suite of utilities for comparing genomic features. *Bioinformatics* **2010**, *26*, 841–842. https://doi.org/10.1093/bioinformatics/btq033.
47. Martin, M.; Patterson, M.; Garg, S.; Fischer, S.O.; Pisanti, N.; Klau, G.W.; Schönhuth, A.; Marschall, T. WhatsHap: Fast and accurate read-based phasing. *bioRxiv* **2016**. https://doi.org/10.1101/085050.
48. Garg, S.; Martin, M.; Marschall, T. Read-based phasing of related individuals. *Bioinformatics* **2016**, *32*, i234–i242. https://doi.org/10.1093/bioinformatics/btw276.
49. Danecek, P.; Bonfield, J.K.; Liddle, J.; Marshall, J.; Ohan, V.; Pollard, M.O.; Whitwham, A.; Keane, T.; McCarthy, S.A.; Davies, R.M.; et al. Twelve years of SAMtools and BCFtools. *GigaScience* **2021**, *10*, giab008. https://doi.org/10.1093/gigascience/giab008.
50. Pedersen, B.S.; Quinlan, A.R. cyvcf2: Fast, flexible variant analysis with Python. *Bioinformatics* **2017**, *33*, 1867–1869. https://doi.org/10.1093/bioinformatics/btx057.
51. Kumar, L.; Futschik, M.E. Mfuzz: A software package for soft clustering of microarray data. *Bioinformation* **2007**, *2*, 5–7. https://doi.org/10.6026/97320630002005.
52. Cantalapiedra, C.P.; Hernández-Plaza, A.; Letunic, I.; Bork, P.; Huerta-Cepas, J. eggNOG-mapper v2: Functional Annotation, Orthology Assignments, and Domain Prediction at the Metagenomic Scale. *Mol. Biol. Evol.* **2021**, *38*, 5825–5829. https://doi.org/10.1093/molbev/msab293.
53. Yu, G.; Wang, L.G.; Han, Y.; He, Q.Y. clusterProfiler: An R Package for Comparing Biological Themes Among Gene Clusters. *OMICS* **2012**, *16*, 284–287. https://doi.org/10.1089/omi.2011.0118.
54. Wickham, H. *ggplot2: Elegant Graphics for Data Analysis*, 2nd ed.; Springer: Cham, Switzerland, 2016.

Disclaimer/Publisher's Note: The statements, opinions and data contained in all publications are solely those of the individual author(s) and contributor(s) and not of MDPI and/or the editor(s). MDPI and/or the editor(s) disclaim responsibility for any injury to people or property resulting from any ideas, methods, instructions or products referred to in the content.